Nonsnaking doubly diffusive convectons and the twist instability

Cédric Beaume,[1,a)] Edgar Knobloch,[1,b)] and Alain Bergeon[2,c)]
[1]*Department of Physics, University of California, Berkeley, California 94720, USA*
[2]*Université de Toulouse, INPT, UPS, IMFT (Institut de Mécanique des Fluides de Toulouse), Allée Camille Soula, F-31400 Toulouse, France and CNRS, IMFT, F-31400 Toulouse, France*

Doubly diffusive convection in a three-dimensional horizontally extended domain with a square cross section in the vertical is considered. The fluid motion is driven by horizontal temperature and concentration differences in the transverse direction. When the buoyancy ratio $N = -1$ and the Rayleigh number is increased the conduction state loses stability to a subcritical, almost two-dimensional roll structure localized in the longitudinal direction. This structure exhibits abrupt growth in length near a particular value of the Rayleigh number but does not snake. Prior to this filling transition the structure becomes unstable to a secondary twist instability generating a pair of stationary, spatially localized zigzag states. In contrast to the primary branch these states snake as they grow in extent and eventually fill the whole domain. The origin of the twist instability and the properties of the resulting localized structures are investigated for both periodic and no-slip boundary conditions in the extended direction.

I. INTRODUCTION

The term doubly diffusive is used to refer to fluid systems where two competing fields diffuse at different rates. As examples we mention the three-component fluid mixture studied by Welander[1] and two-component convection in a horizontal layer with competing temperature and concentration fields driven by imposed temperature and concentration differences.[2] In such configurations doubly diffusive effects may generate instabilities even when the mixture is stably stratified. When the temperature is stabilizing (i.e., a hot fluid overlies a cold fluid) while the concentration is destabilizing (i.e., the heavier component overlies the lighter one) the instability leads to a fingering instability in which the sinking (respectively, rising) fingers carry the heavier (respectively, lighter) component of the mixture. This instability plays an important role in ocean dynamics, particularly in equatorial regions,[3,4] as well as in astrophysics.[5,6] On the other hand, when the concentration is stabilizing while the temperature gradient is destabilizing, oscillatory or overstable dynamics are typically observed, and these may lead to the formation of well-mixed diffusive layers. This type of instability is also found in astrophysics[7] and in oceanography,[8] albeit at higher latitudes. Doubly diffusive instabilities with misaligned gradients are common in solidification processes[9] and the case of horizontal gradients is considered representative.[10–12] In the oceans the presence of icebergs may incline dramatically both the temperature and concentration gradients, a situation that may be idealized in the form of a vertical interface between the cold and pure water of the iceberg and the warm and salty water of the ocean.[13] The flow that results is referred to as natural doubly diffusive convection.

Doubly diffusive convection is known to exhibit a great variety of behavior. A number of studies have examined the standing and traveling waves characteristic of the overstable regime and the

a)ced.beaume@gmail.com
b)knobloch@berkeley.edu
c)alain.bergeon@imft.fr

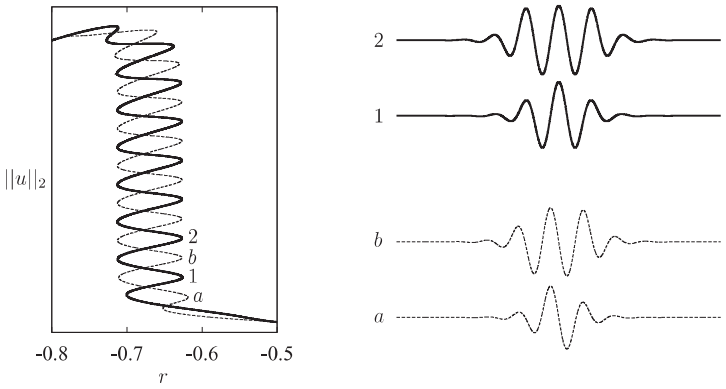

FIG. 1. Bifurcation diagram based on Ref. 24 showing the L_2 norm of stationary localized solutions $u(x)$ of Eq. (1) in a periodic domain of period 20π as a function of r when $\nu = 2$. The localized structures are homoclinic orbits to the trivial state $u = 0$ passing near a periodic state and lie on a pair of snaking branches.

associated chaotic oscillations.[14–16] Recent work has focused on spatially localized convection first observed by Ghorayeb and Mojtabi[17] in natural doubly diffusive convection. Since then stationary localized convection has been extensively studied in two-dimensional (2D) doubly diffusive convection in a horizontal layer, both with Soret effect[18–20] and without.[21,22] Solutions of this type, hereafter referred to as convectons, may be viewed as homoclinic orbits in space connecting the conduction state to itself and are associated with heteroclinic orbits or fronts connecting the conduction state to a periodic roll state and back again. These solutions have recently been computed in natural three-dimensional (3D) doubly diffusive convection in a vertically extended cavity[23] and are accompanied by secondary instabilities leading to the twisting of some of the convection rolls, an instability only allowed by the additional freedom provided by the third dimension. The present paper examines the same system, but this time focusing on a horizontally extended cavity. The study identifies both similarities and key differences between these two systems.

Localization phenomena are easier to apprehend using the cubic-quintic Swift–Hohenberg (SH35) equation on the real line[24]

$$\partial_t u = ru - (1 + \partial_{xx}^2)^2 u + \nu u^3 - u^5. \tag{1}$$

Here $u(x, t)$ is a scalar field, r is a bifurcation parameter, and ν is a real coefficient. With periodic boundary conditions the equation is translation-invariant in x and spatially reversible with respect to $x \to -x$, $u \to \pm u$, and admits a trivial solution $u \equiv 0$. The equation has, moreover, variational dynamics,

$$\frac{\partial u}{\partial t} = -\frac{\delta F}{\delta u}, \tag{2}$$

with the free energy

$$F \equiv \frac{1}{L}\int_0^L \left(-\frac{1}{2}ru^2 + \frac{1}{2}[(1 + \partial_{xx}^2)u]^2 - \frac{1}{4}\nu u^4 + \frac{1}{6}u^6\right) dx, \tag{3}$$

where $L < \infty$ is the imposed spatial period, implying that all solutions evolve towards stationary states as $t \to \infty$. The Swift–Hohenberg equation (1) contains homoclinic orbits to the trivial solution $u = 0$ resembling those observed in doubly diffusive convection, i.e., consisting of a periodic roll state embedded in a background homogeneous state. The localized solutions of the equation (like those of the doubly diffusive problem) lie on a pair of intertwined branches corresponding to states of even and odd parity. As one follows each branch the solution repeatedly adds new rolls at either end, a process reflected in the "snaking" behavior of the two branches (Fig. 1), itself a consequence of the pinning of the front connecting the trivial and periodic states to the periodic pattern behind it. Details of this process are described in Refs. 25 and 26.

The symmetry $u \to -u$ plays an important role in the behavior of SH35[24] and corresponds to the reflection symmetry $S_\triangle$ of the fluid equations as discussed below. To interpret the solutions of SH35 in a fluid dynamical context the order parameter u is to be identified with the temperature fluctuation or vertical velocity in the layer midplane.

The paper is organized as follows. In Sec. II we present the mathematical formulation of the problem, followed in Sec. III by the results in the case of closed container boundary conditions. Section IV reports on the differences observed when periodic boundary conditions are imposed in the extended direction. The paper concludes with a brief discussion in Sec. V.

II. MATHEMATICAL FORMULATION

We consider a binary fluid placed within horizontal gradients of temperature and concentration. These gradients are introduced via Dirichlet boundary conditions applied on opposite vertical walls at $y = 0, l$. The rear wall at $y = 0$ is maintained at fixed temperature $T^* = T_r$ and concentration in the heavier component $C^* = C_r$ while the front wall at $y = l$ is maintained at temperature $T^* = T_r + \triangle T$ and concentration $C^* = C_r + \triangle C$, with $\triangle T > 0$ and $\triangle C > 0$. We nondimensionalize the equations using l for lengths, $\triangle T$ for the temperature, $\triangle C$ for the concentration, and l^2/κ for the time, where l^2 is the area of the square cross-section and κ is the thermal diffusivity. Cross-diffusion effects are neglected. The Boussinesq approximation allows us to expand the fluid density about the reference values T_r and C_r,

$$\rho(T^*, C^*) = \rho_0 + \rho_T(T^* - T_r) + \rho_C(C^* - C_r), \tag{4}$$

where ρ_0 is the fluid density at the reference temperature T_r and concentration C_r, and $\rho_T < 0$ and $\rho_C > 0$ denote the thermal and solutal "expansion" coefficients at T_r and C_r. Departures of the temperature and concentration from T_r and C_r generate buoyancy forces given by $F_T = -\rho_T g(T^* - T_r)\hat{\mathbf{z}}$ and $F_C = -\rho_C g(C^* - C_r)\hat{\mathbf{z}}$, respectively. Here g is the gravitational acceleration and $\hat{\mathbf{z}}$ denotes the unit vector in the vertical direction. We define the buoyancy ratio N, quantifying the ratio of the two contributions to the buoyancy force, according to

$$N = \frac{\rho_C \triangle C}{\rho_T \triangle T}. \tag{5}$$

In the following we restrict our attention to the case $N = -1$, for which the thermal and solutal forces compete but balance. This assumption yields a system with a trivial solution in which the fluid is motionless and the temperature and concentration fields are linear. For other values of N the trivial state is replaced by a large scale convection flow.

We describe the system using the Navier–Stokes equation for an incompressible flow $\mathbf{u} \equiv u\hat{\mathbf{x}} + v\hat{\mathbf{y}} + w\hat{\mathbf{z}}$ coupled to equations describing advection and diffusion of the temperature and concentration fields. The nondimensionalized equations read

$$Pr^{-1}[\partial_t \mathbf{u} + (\mathbf{u} \cdot \nabla)\mathbf{u}] = -\nabla p + Ra(T - C)\hat{\mathbf{z}} + \nabla^2 \mathbf{u}, \tag{6}$$

$$\nabla \cdot \mathbf{u} = 0, \tag{7}$$

$$\partial_t T + (\mathbf{u} \cdot \nabla)T = \nabla^2 T, \tag{8}$$

$$\partial_t C + (\mathbf{u} \cdot \nabla)C = \tau \nabla^2 C, \tag{9}$$

where p is the pressure and we have written $T = (T^* - T_r)/\triangle T$, $C = (C^* - C_r)/\triangle C$. Owing to our choice of nondimensionalization, three nondimensional parameters are introduced, namely, the Rayleigh number Ra, the Prandtl number Pr, and the (inverse) Lewis number τ:

$$Ra = \frac{g|\rho_T|\triangle T l^3}{\nu\kappa}, \qquad Pr = \frac{\nu}{\kappa}, \qquad \tau = \frac{D}{\kappa}, \tag{10}$$

where ν is the kinematic viscosity and D is the concentration diffusivity.

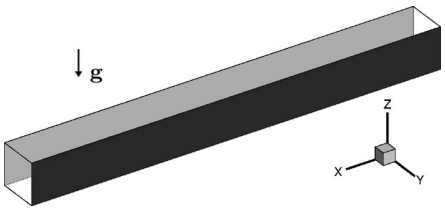

FIG. 2. Sketch of the horizontally extended domain. The boundary conditions on the square cross-section are no-slip, with no-flux conditions for the temperature and concentration on the z-walls, $T = C = 0$ at $y = 0$ (section represented in light gray) and $T = C = 1$ at $y = 1$ (section represented in dark gray). The boundary conditions on the x-walls may be either periodic or no-slip/no-flux.

The fluid is confined within a domain of square cross-section, extended in the $\hat{\mathbf{x}}$ direction as sketched in Fig. 2, and subject to the boundary conditions

$$\text{at } y = 0: \qquad u = v = w = T = C = 0, \tag{11}$$

$$\text{at } y = 1: \qquad u = v = w = T - 1 = C - 1 = 0, \tag{12}$$

$$\text{at } z = \{0, 1\}: \qquad u = v = w = \partial_z T = \partial_z C = 0. \tag{13}$$

We use two sets of boundary conditions at $x = 0, L$, where $L \gg 1$ is the nondimensional length of the enclosure in the horizontal direction, closed container boundary conditions (CCBC),

$$\text{at } x = \{0, L\}: \qquad u = v = w = \partial_x T = \partial_x C = 0, \tag{14}$$

and periodic boundary conditions (PBC) at $x = 0, L$. In both cases, Eqs. (6)–(9) with the corresponding boundary conditions admit a conduction solution $(u, v, w, T, C) = (0, 0, 0, y, y)$. The symmetry properties of the flow that results from the loss of stability of this state are found by setting $\Theta = T - y$ and $\Sigma = C - y$. Since the buoyancy force lies in the vertical direction the system is equivariant under the following reflections:

$$S_x : (x, y, z) \to (L - x, y, z), \quad (u, v, w, \Theta, \Sigma) \to (-u, v, w, \Theta, \Sigma), \tag{15}$$

$$S_\triangle : (x, y, z) \to (x, 1 - y, 1 - z), \quad (u, v, w, \Theta, \Sigma) \to -(-u, v, w, \Theta, \Sigma). \tag{16}$$

It follows that with closed container boundary conditions, the equations are D_2-equivariant,[27] with $D_2 = \{\mathcal{I}, S_x, S_\triangle, S_c\}$, where $\mathcal{I}$ is the identity operator and $S_c = S_x \circ S_\triangle = S_\triangle \circ S_x$ represents centro-symmetry. With periodic boundary conditions, the system is also equivariant with respect to continuous translations T_x in x modulo the period L. The system is now equivariant with respect to a different symmetry group: $O(2) \times Z_2$, where $O(2) = \{\mathcal{I}, S_x, T_x\}$ and $Z_2 = \{\mathcal{I}, S_\triangle\}$.[27] The consequences of this change in symmetry are substantial and are discussed below.

The equations are solved for the same parameters as used in Ref. 23, viz., $Pr = 1$ and $\tau = 1/11$. To allow localized solutions to develop in the domain we choose a large aspect ratio domain, $L = 21$. We compute bifurcation diagrams by finding stationary solutions of Eqs. (6)–(9) with the corresponding boundary conditions using a continuation method based on a Newton solver as described in Mamun and Tuckerman.[28,29] The time-stepping scheme used is described in Karniadakis *et al.*[30] and the spatial discretisation employs a spectral element method. Further details of the numerical method can be found in Ref. 31. The calculations are carried out using 21 spectral elements each with $13 \times 17 \times 17$ Gauss–Lobatto–Legendre nodes.

III. CLOSED CONTAINER

We now describe the bifurcation scenario obtained with closed container boundary conditions. Owing to the confinement in the vertical direction, the first instability cannot develop as easily as in

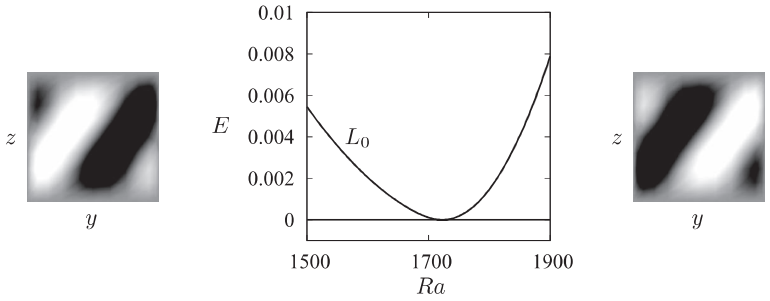

FIG. 3. Bifurcation diagram for CCBC showing the vicinity of the primary bifurcation from the conduction state, $Ra \approx 1719$, in terms of the kinetic energy E as a function of the Rayleigh number Ra. The bifurcation is transcritical and generates two branches of solutions. Of these, the subcritical branch L_0 contains localized states while the supercritical branch consists of spatially extended states. The left ($Ra \approx 1649$) and right ($Ra \approx 1771$) panels show, respectively, the isovalues of the vertical velocity w in the central cross-section on the subcritical and supercritical parts of the L_0 branch, dark (light) shading indicating positive (negative) velocity.

vertically extended domains.[32] Thus the first bifurcation from the conduction state occurs at a larger Rayleigh number, $Ra \approx 1719$, a value similar to the 2D result $Ra \approx 1717.24$.[33] This bifurcation, shown in Fig. 3, is transcritical and generates the (subcritical) branch L_0 of localized solutions shown in Fig. 4(a). Snapshots taken along L_0 are shown in Fig. 5. The figure shows that the growth of the instability leads to a single roll localized at the center of the domain. The no-slip boundary conditions suppress the growth near $x = 0, L$ and the resulting modulation increases rapidly with decreasing Ra leading to a strongly localized state by the time Ra reaches $Ra \approx 746$. By this point, the amplitude of the convection has reached saturation and the structure begins to lengthen again. As a result, its energy undergoes a rapid increase but no snaking takes place. This is because the structure between the fronts on either side is spatially homogeneous – fronts cannot pin to a homogeneous state. Once the structure almost fills the enclosure the growth phase terminates and the branch turns towards larger values of Ra. Thus the localized states turn continuously into a spatially extended structure of almost uniform amplitude except for the vicinity of the endwalls at $x = 0, L$. As described by Mercader *et al.*[18] this is a consequence of the no-slip boundary conditions imposed at the end walls.

Supercritical secondary instabilities occur along the *lower* part of L_0 at $Ra \approx 1224$ and $Ra \approx 1226$ (bifurcations not shown). The marginal modes responsible for these instabilities both break $S_\triangle$ and hence create pitchforks. The resulting branches are labeled L_0^- and L_0^+ in Fig. 4(b). The former branch breaks S_c but remains S_x-symmetric while the latter breaks S_x but preserves S_c.

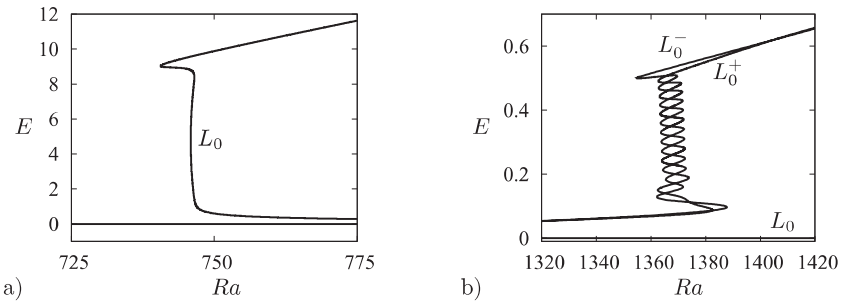

FIG. 4. Bifurcation diagrams for CCBC showing the kinetic energy E as a function of the Rayleigh number Ra for (a) the L_0 branch and (b) the secondary branches L_0^- and L_0^+ that bifurcate from L_0 at $Ra \approx 1224$ and $Ra \approx 1226$, respectively.

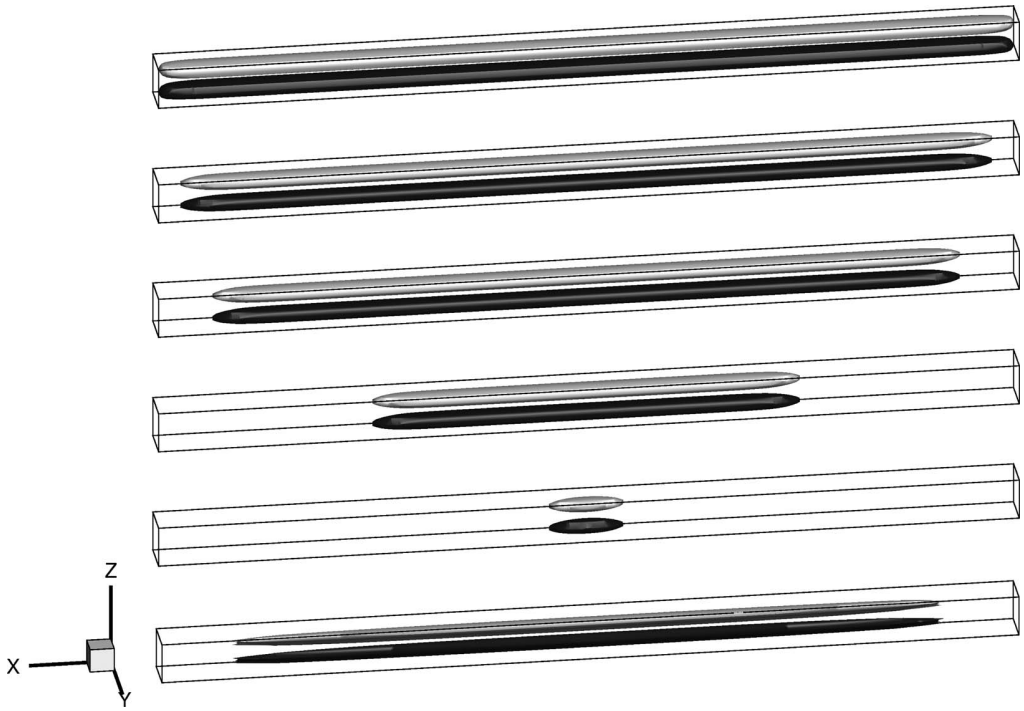

FIG. 5. Snapshots of localized states on the L_0 branch. From bottom to top: representation of the marginal eigenmode and of the solution at $Ra \approx 752$, followed by the solutions at each of the three saddle-nodes, ending with the solution at $Ra \approx 851$ along the upper part of the branch. The flow is represented using two isovalues of the y velocity, $v = \pm V$, with V chosen appropriately (light indicates $v = -V < 0$ while dark indicates $v = V > 0$). A different value of V is used for the marginal eigenmode in the lowest panel.

Both L_0^- and L_0^+ undergo snaking between $Ra \approx 1363$ and $Ra \approx 1374$ before turning supercritical and hence are similar to the secondary snaking branches described in Ref. 23. Figure 6 shows the L_0 solution at bifurcation (lowest panels) followed by the solutions $L_0^{\mp}$ at successive saddle-nodes in the snaking region. Since the secondary instability takes place on the lower part of the L_0 branch the bifurcating solutions take the form of a strongly localized but weak convective structure. This structure consists of a single roll with upflow near the $y = 1$ wall and downflow near $y = 0$. With increasing Ra, this roll splits. Along L_0^- the upflow region splits into two upflow regions separated by a region of weak upflow while the downflow region remains essentially unchanged. At the same time the u velocity builds up inside the virtually two-dimensional convective structure while v oscillates in x (compare the middle panel of Fig. 7 with Fig. 5). The combination of these effects twists the primary roll around the vertical axis by a finite angle by the time the system reaches the first saddle-node (Fig. 4(b)) as represented in the second panel from bottom in Fig. 6(a). Thereafter the structure nucleates twisted rolls on either side in the usual fashion and the structure grows until the enclosure is filled (Fig. 6(a)). Thus all L_0^- states contain an even number of twisted rolls (Fig. 7) and the growth of the structure is associated with front pinning and hence snaking. During this growth process the axes of the cells remain horizontal but rotate about the vertical axis and this rotation alternates from one roll to the next, generating a zigzag array of convection cells. Figure 7 reveals the twisted character of the L_0^- solution in terms of the three velocity fields u, v, and w.

In contrast, the break-up process along the L_0^+ branch leads instead to states with an odd number of convection cells (Fig. 6(b)) but with a similar zigzag structure. Once the enclosure is filled (this occurs with 18 cells on L_0^- and 17 cells on L_0^+) both branches exit the snaking region and transform continuously into larger amplitude branches of almost periodic states. However, all of these states have very small energy relative to the corresponding states on the upper part of the L_0 branch. Both L_0^- and L_0^+ branches are unstable.

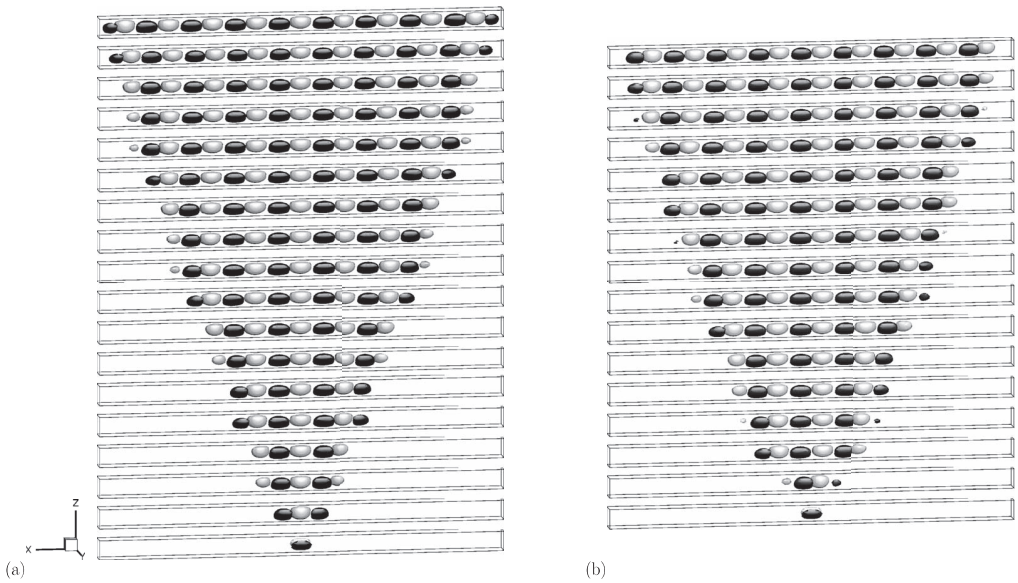

FIG. 6. Snapshots of the localized states lying on (a) the L_0^- branch and (b) the L_0^+ branch. From bottom to top: representation of the solution at the branching point on L_0 followed by the solutions at each subsequent saddle-node along the branch and ending with a solution taken on the upper part of the snaking branch at $Ra \approx 1380$. The flow is represented by two isovalues of the z velocity, $w = \pm W$, with W chosen appropriately (light indicates $w = -W < 0$ while dark indicates $w = W > 0$).

IV. PERIODIC DOMAIN

It is of interest to compare the above results with the corresponding results for periodic boundary conditions in the $\hat{\mathbf{x}}$ direction. The change in the boundary condition preserves the conduction solution but the corresponding primary instability now creates a strictly two-dimensional convection roll that is invariant in the $\hat{\mathbf{x}}$ direction. This T_x-invariant solution does not break any of the symmetries of the system and is, therefore, created through a transcritical bifurcation at $Ra \approx 1716.2$. The bifurcation generates a stable supercritical branch and a once unstable subcritical branch. We focus here on the latter.

Figure 8 represents the bifurcation diagram for the subcritical branch and compares it to the results from Sec. III. The subcritical branch of x-invariant states, called H^x, turns around at a saddle-node at $Ra \approx 676$ before extending to large energy at high Rayleigh numbers. Along this branch, a T_x-breaking bifurcation occurs at small amplitude creating a branch L_0^x of spatially modulated states. As one moves away from the bifurcation point, the modulation strengthens, forming a pair of fronts that localize the solution in space. The branch L_0^x follows the same evolution as its analogue L_0 in the closed container case, growing in energy in the vicinity of $Ra \approx 746$ (Fig. 8). At the lower end the solutions consist of a single roll localized in the center of the domain. This roll expands continuously

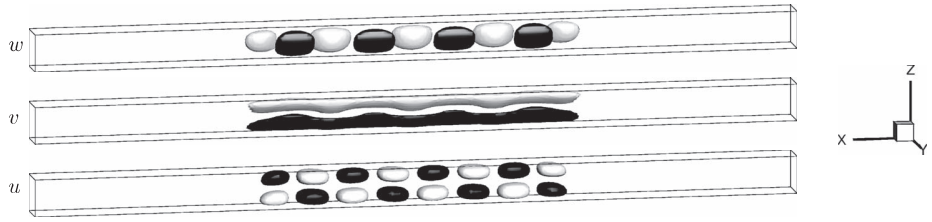

FIG. 7. An L_0^- solution at $Ra = 1364$ in terms of the three velocity fields u, v, and w. In each panel the representation uses equal and opposite contour values, the light (dark) color indicating negative (positive) velocity. For this solution the maximum values of u, v, and w are $u_{max} \approx 0.40$, $v_{max} \approx 0.23$, and $w_{max} \approx 0.62$.

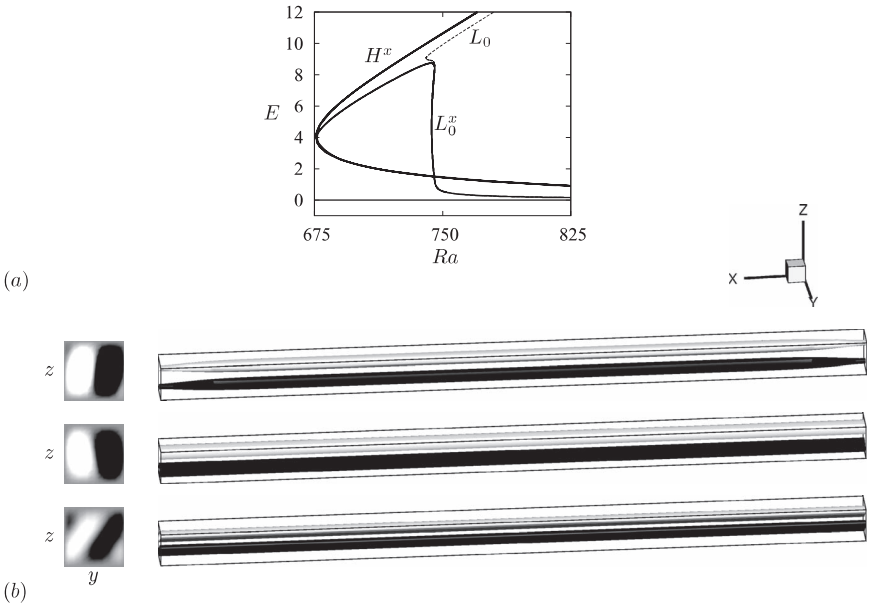

FIG. 8. (a) Bifurcation diagram representing the kinetic energy E as a function of the Rayleigh number Ra along branch L_0 (dashed line) for a closed container, and H^x and L_0^x (solid lines) for a periodic container. The branch H^x bifurcates from the conduction solution $E = 0$ and consists of solutions invariant in the x direction. The branch L_0^x of localized states bifurcates from H^x and is similar to the branch L_0 in the closed container, but unlike L_0 it terminates on H^x close to its saddle-node instead of extending towards higher Rayleigh numbers. (b) From bottom to top: snapshot along H^x at $Ra \approx 1485$ (lower part of H_0^x), at $Ra \approx 1462$ (upper part of H^x) and along L_0^x at $Ra \approx 685$. Left slices represent isovalues of the vertical velocity w in the plane $x = L/2$ while the right snapshots represent isosurfaces of opposite values of the y-velocity (dark: $v > 0$, light: $v < 0$).

in the x direction as the branch grows in energy, much as the corresponding solutions in Fig. 5. Near the top of the branch, the roll state has expanded to fill the domain and subsequent evolution depends on the boundary conditions at $x = 0, L$. With no-slip boundary conditions, defects are present at either boundary (Fig. 5) and L_0 turns towards larger Rayleigh numbers and larger amplitudes. In contrast, with periodic boundary conditions no defects are created (after all, the domain is translation-invariant in the x direction) and L_0 instead turns towards smaller Rayleigh numbers and terminates on the two-dimensional state H^x close to its saddle-node. This is as expected since it is known that a branch of spatially modulated states bifurcates from folds of spatially homogeneous states.[34]

It is noteworthy that the branch L_0^x follows L_0 very closely during its abrupt growth phase, i.e., while the solutions remain localized away from the boundaries (Fig. 8). With PBC the first tertiary bifurcations from L_0^x are located at $Ra \approx 1218$ (L_0^{x-}) and $Ra \approx 1220$ (L_0^{x+}) and these create branches $L_0^{x\mp}$ of twisted rolls (Fig. 9(a)). Like the corresponding bifurcations from L_0 (at $Ra \approx 1224$ (L_0^-) and $Ra \approx 1226$ (L_0^+)) these branches consist of S_x-symmetric (respectively, S_c-symmetric) solutions and track closely the corresponding solutions L_0^- (respectively, L_0^+) with no-slip boundary conditions. Once again this is a consequence of the localized nature of these solutions. However, differences appear once the solutions have grown to fill the domain, i.e., near the top of the snaking regime. At this point, the branches $L_0^{x\mp}$ of localized twisted states exit the snaking region but instead of turning into large amplitude states like $L_0^{\mp}$, they turn towards smaller Rayleigh numbers and terminate together at $Ra \approx 1269$ on a new branch of spatially periodic states referred to as P^x (Fig. 9(b)). These states take the form of a zigzag array of 20 twisted rolls within the domain (Fig. 10) and bifurcate from the branch of x-invariant states H^x at $Ra \approx 1211$. This bifurcation breaks the x-invariance of the solution by twisting the roll around the vertical axis and is a subcritical pitchfork of revolution since it bifurcates backwards relative to the direction of increasing instability. The twist oscillates with x with a wavelength determined by the instability, resulting in an array of 20 rolls, each twisted in the opposite sense from its neighbors. The termination of the $L_0^{x\mp}$ branches on P^x corresponds to a local

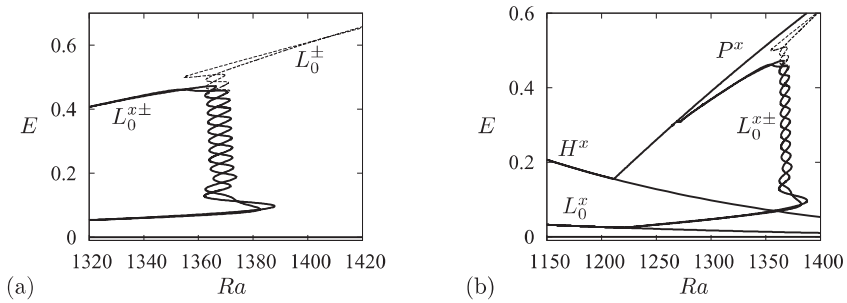

FIG. 9. (a) Bifurcation diagram representing the kinetic energy E as a function of the Rayleigh number Ra for the branches of twisted localized states with no-slip ($L_0^{\pm}$, dashed lines) and periodic ($L_0^{x\pm}$, full lines) boundary conditions. (b) Bifurcation diagram for the twisted localized states $L_0^{x\pm}$ with PBC: $L_0^{x\pm}$ emerge from a branch of homogeneous localized states L_0^x and terminate on a branch of periodic twisted states P^x. The latter bifurcates from the branch H^x of 2D states connecting P^x and L_0^x.

bifurcation of the P^x state leading to spatial modulation of the P^x state on the scale of the domain and agrees with the results of linear stability analysis of the P^x state, viz., $Ra \approx 1269$. However, the P^x state is unstable on either side of this termination point, owing to the presence of other unstable eigenvalues.

V. DISCUSSION

We have computed in this paper two new types of convectons in natural doubly diffusive convection. These solutions are present in a horizontally extended domain with a square cross-section driven by imposed temperature and concentration differences in the horizontal. The first type is a localized, almost two-dimensional structure bounded by a pair of fronts connecting the structure to the conduction state, resembling a two-dimensional roll state with axis along the extended direction. Since both states are spatially homogeneous in the extended direction no front pinning takes place and snaking is, therefore, absent. States of this type expand abruptly in the extended direction near a special point in parameter space corresponding to the formation of a pair of heteroclinic connections between two different fixed points in a spatial dynamics view of the system.[26] This point, variously referred to as the nonsnaking[35] or protosnaking[36] point plays the role of a Maxwell point in systems, like the Swift-Hohenberg equation (1), with gradient dynamics. If the spatial eigenvalues of one of the fixed points are complex the resulting behavior may be termed collapsed snaking.[37] Figure 11 shows an example of this type of behavior. The figure reveals the presence of a parameter value at which the two coexisting homogeneous states have the same free energy F. As neither state is associated with an intrinsic wavelength fronts between them can be placed in arbitrary positions without changing the value of the functional F. Thus states of arbitrarily large size are all present at a single value of the bifurcation parameter. The two-dimensional roll state computed here follows the same behavior despite the absence of a free energy for the governing equations, and does so until it reaches a size comparable to the domain size. When the boundaries are no-slip the localized

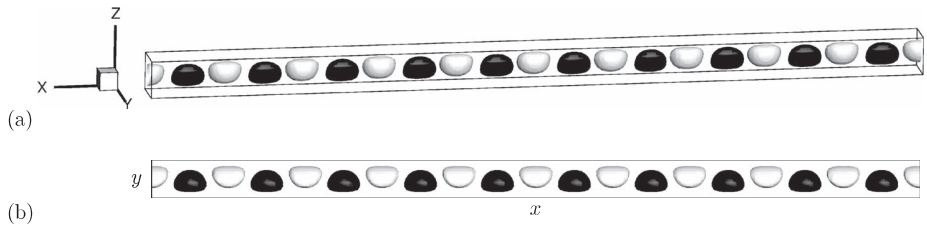

FIG. 10. Periodic solution P^x at $Ra \approx 1600$ consisting of a zigzag pattern of twisted rolls, visualized using two opposite values of the z component of the velocity w. (a) A three-dimensional rendering. (b) Top view showing the twist from a better angle.

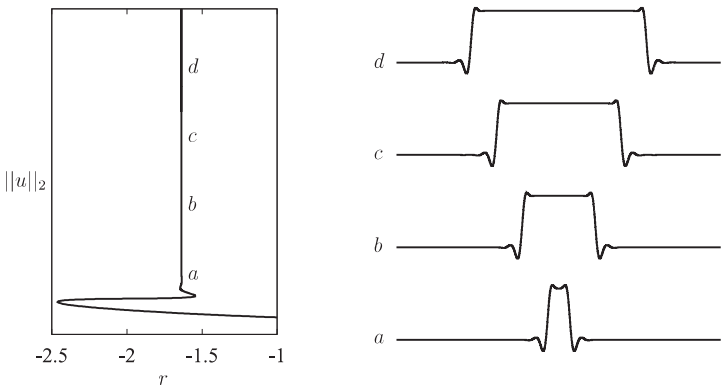

FIG. 11. Same as Fig. 1 but showing collapsed snaking in a 40π domain when $\nu = 3.75$. The localized structures are fronts connecting two distinct homogeneous states and lie on a branch that grows vertically as the nontrivial state $u \neq 0$ invades the domain.

state turns continuously into an extended domain-filling state with defect-like structure at the walls; when periodic boundary conditions are used the defects are absent and the localized states instead terminate on the branch of two-dimensional states. This is as expected since the no-slip boundaries destroy the two-dimensional state.[18,20]

The same process is repeated for the second type of convecton, the localized twisted states that are produced in tertiary bifurcations from the two-dimensional localized states. Once again, with no-slip boundary conditions the localized states change continuously into extended domain-filling states once they reach the size of the domain, again with defects at the walls. In contrast, with periodic boundary conditions these states instead turn towards smaller Rayleigh numbers and terminate on a periodic state, this time the zigzag twisted roll state. Thus the main difference between these two convecton types is the nonsnaking behavior of the first type and the snaking behavior of the second type. Of course, the latter is the result of pinning of the fronts that bound the convecton to the spatial structure in between and is a direct consequence of the twist instability – without a finite angle twist no pinning would be present and no snaking would take place.

The presence of the tertiary twist instability should come as no surprise. Similar bifurcations are present in a vertically extended domain[23] and reflect the presence of a related three-dimensional instability present in small domains with no-slip boundary conditions, as described in Ref. 31. Figure 12 summarizes our results for periodic boundary conditions. The figure highlights an important fact: the secondary twist bifurcation generating the periodic branch P^x destabilizes the branch H^x at lower Rayleigh numbers. As a result the H^x branch is (at least) three times unstable below this bifurcation and since only two eigenvalues restabilize (one at the termination of L_0^x and the other at the fold) the H^x branch remains unstable to the twist mode even above the fold. In Ref. 31 this fact was found to be responsible for the presence of temporal oscillations in a small aspect ratio domain with no-slip boundaries everywhere. These oscillations may be chaotic and appear in the system as a result of a global bifurcation. We have looked for similar behavior in the present system, using direct numerical integration of the governing equations with periodic boundary conditions in the extended dimension, but found none. We believe this to be the consequence of the small extent in the vertical direction that constrains the dynamics and forces the solutions to evolve towards the stable solution lying on the supercritical branch created at the primary instability. To our knowledge this is the first example of a system exhibiting subcritical branches in which the trivial (conduction) solution appears to be a global attractor all the way until the onset of the primary instability – although other systems come close.[38]

There remains an important issue. As shown in Figs. 4(b) and 9(a) the tertiary snaking of the twisted localized states in the PBC case coincides almost exactly with the secondary snaking with no-slip boundary conditions. As already mentioned this is a consequence of the localization of the structures away from the boundaries. However, the snaking structure is slightly inclined towards lower Rayleigh numbers, and this inclination is the same for both sets of boundary conditions, thereby

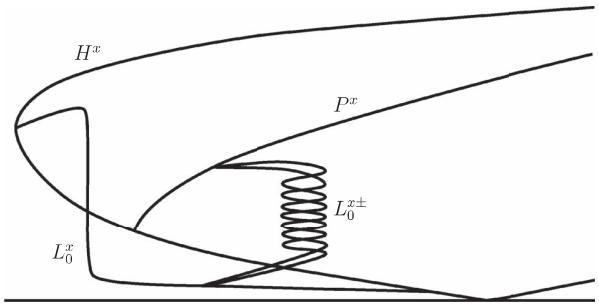

FIG. 12. Sketch of the bifurcation scenario for periodic boundary conditions in the extended direction. A typical integral quantity such as the kinetic energy is represented against the Rayleigh number. The bifurcation diagram has been stretched for convenience and is not to scale. Representative solutions along H^x, P^x, and $L_0^{x\pm}$ are shown in Figs. 8(b) and 10, and 6, respectively, while those along L_0^x resemble those in Fig. 5.

excluding boundary effects as a possible explanation. We believe instead that it is a consequence of the weakly three-dimensional structure of the fronts at either end of the structure associated with weak outward expulsion of concentration gradients. The flow in this region moves the concentration around the axis of the domain alternately sampling fixed flux and fixed concentration boundary conditions. The former enhances concentration pumping[39] while the latter suppresses pumping.[22] Residual concentration pumping is, therefore, likely to be present and its presence will *reduce* the background concentration gradient sensed by the convecton. We expect this effect to be proportional to the square of the amplitude of convection and hence linear in the Rayleigh number. In other words, we predict a linear slant of the snaking structure towards lower Rayleigh numbers, independent of the boundary conditions, as observed in the numerically generated bifurcation diagrams.

The physical parameters used in the present study are the same as in Ref. 23 and it is therefore of interest to compare the two systems. The domain used in Ref. 23 has a square cross-section in the horizontal and is extended in the vertical direction. In the aforementioned paper the authors found convectons consisting of rolls with horizontal axes exhibiting localization in the vertical direction. In some of these the roll axes are perpendicular to the lateral walls, but in others the axes are rotated in the horizontal direction with the direction of rotation switching from roll to roll, forming a zigzag structure. Solutions of the former type are organized into primary snaking branches while the latter form secondary snaking branches. Thus the vertically extended system exhibits similar states to those found here in the horizontally extended system. In both cases the novel localized structures are present in a Rayleigh number interval straddling $Ra \approx 750$ although the primary snake is replaced here by a collapsed snake, a consequence of the near two-dimensionality of the convectons in this regime. Of course, once fully three-dimensional instabilities set in, snaking occurs in the latter case as well although it does so at larger values of the Rayleigh number. Based on these results we anticipate a yet richer variety of localized structures in a horizontally extended cavity with a square cross-section in the horizontal. This geometry will be the subject of future work.[40]

ACKNOWLEDGMENTS

This work was supported in part by a Chaire d'Excellence Pierre de Fermat de la région Midi-Pyrénées (E.K.) and by the National Science Foundation under Grant No. DMS-1211953 (C.B. and E.K.).

[1] P. Welander, "A new type of double-diffusive instability?" Tellus **41A**, 66–72 (1989).
[2] R. W. Schmitt, "Double diffusion in oceanography," Annu. Rev. Fluid Mech. **26**, 255–285 (1994).
[3] M. E. Stern, "Collective instability of salt fingers," J. Fluid Mech. **35**, 209–218 (1969).
[4] T. Radko, "What determines the thickness of layers in a thermohaline staircase?," J. Fluid Mech. **523**, 79–98 (2005).
[5] E. Knobloch, "Nonlinear diffusive instabilities in differentially rotating stars," Geophys. Astrophys. Fluid Dyn. **22**, 133–158 (1982).
[6] J. M. Brown, P. Garaud, and S. Stellmach, "Chemical transport and spontaneous layer formation in fingering convection in astrophysics," Astrophys. J. **768**, 34 (2013).

[7] E. Rosenblum, P. Garaud, A. Traxler, and S. Stellmach, "Turbulent mixing and layer formation in double-diffusive convection: Three-dimensional numerical simulations and theory," Astrophys. J. **731**, 66 (2011).
[8] D. E. Kelley, H. J. S. Fernando, A. E. Gargett, J. Tanny, and E. Özsoy, "The diffusive regime of double diffusive convection," Prog. Oceanogr. **56**, 461–481 (2003).
[9] W. R. Wilcox, "Transport phenomena in crystal growth from solution," Prog. Cryst. Growth Charact. Mater. **26**, 153–194 (1993).
[10] N. Tsitverblit and E. Kit, "The multiplicity of steady flows in confined double-diffusive convection with lateral heating," Phys. Fluids A **5**, 1062–1064 (1993).
[11] N. Tsitverblit, "Bifurcation phenomena in confined thermosolutal convection with lateral heating: Commencement of the double-diffusive region," Phys. Fluids **7**, 718–736 (1995).
[12] S. Xin, P. Le Quéré, and L. S. Tuckerman, "Bifurcation analysis of double-diffusive convection with opposing horizontal thermal and solutal gradients," Phys. Fluids **10**, 850–858 (1998).
[13] H. E. Huppert and J. S. Turner, "Ice blocks melting into a salinity gradient," J. Fluid Mech. **100**, 367–384 (1980).
[14] D. R. Moore, J. Toomre, E. Knobloch, and N. O. Weiss, "Period doubling and chaos in partial differential equations for thermosolutal convection," Nature (London) **303**, 663–667 (1983).
[15] E. Knobloch, D. R. Moore, J. Toomre, and N. O. Weiss, "Transition to chaos in two-dimensional double-diffusive convection," J. Fluid Mech. **166**, 409–448 (1986).
[16] A. E. Deane, E. Knobloch, and J. Toomre, "Traveling waves and chaos in thermosolutal convection," Phys. Rev. A **36**, 2862–2869 (1987).
[17] K. Ghorayeb and A. Mojtabi, "Double diffusive convection in a vertical rectangular cavity," Phys. Fluids **9**, 2339–2348 (1997).
[18] I. Mercader, O. Batiste, A. Alonso, and E. Knobloch, "Localized pinning states in closed containers: Homoclinic snaking without bistability," Phys. Rev. E **80**, 025201 (2009).
[19] I. Mercader, O. Batiste, A. Alonso, and E. Knobloch, "Convectons in periodic and bounded domains," Fluid Dyn. Res. **42**, 025505 (2010).
[20] I. Mercader, O. Batiste, A. Alonso, and E. Knobloch, "Convectons, anticonvectons and multiconvectons in binary fluid convection," J. Fluid Mech. **667**, 586–606 (2011).
[21] A. Bergeon and E. Knobloch, "Spatially localized states in natural doubly diffusive convection," Phys. Fluids **20**, 034102 (2008).
[22] C. Beaume, A. Bergeon, and E. Knobloch, "Homoclinic snaking of localized states in doubly diffusive convection," Phys. Fluids **23**, 094102 (2011).
[23] C. Beaume, A. Bergeon, and E. Knobloch, "Convectons and secondary snaking in three-dimensional natural doubly diffusive convection," Phys. Fluids **25**, 024105 (2013).
[24] J. Burke and E. Knobloch, "Snakes and ladders: Localized states in the Swift–Hohenberg equation," Phys. Lett. A **360**, 681–688 (2007).
[25] J. Burke and E. Knobloch, "Homoclinic snaking: Structure and stability," Chaos **17**, 037102 (2007).
[26] D. Avitabile, D. J. B. Lloyd, J. Burke, E. Knobloch, and B. Sandstede, "To snake or not to snake in the planar Swift–Hohenberg equation," SIAM J. App. Dyn. Syst. **9**, 704–733 (2010).
[27] J. D. Crawford and E. Knobloch, "Symmetry and symmetry-breaking bifurcations in fluid mechanics," Annu. Rev. Fluid Mech. **23**, 341–387 (1991).
[28] L. S. Tuckerman, "Steady-state solving via Stokes preconditioning: Recursion relations for elliptic operators," in *11th International Conference on Numerical Methods in Fluid Dynamics*, Lecture Notes in Physics Vol. 323, edited by D. Dwoyer, M. Hussaini, and R. Voigt (Springer, Berlin, 1989), pp. 573–577.
[29] C. K. Mamun and L. S. Tuckerman, "Asymmetry and Hopf bifurcation in spherical Couette flow," Phys. Fluids **7**, 80–91 (1995).
[30] G. E. Karniadakis, M. Israeli, and S. A. Orszag, "High-order splitting methods for the incompressible Navier–Stokes equations," J. Comput. Phys. **97**, 414–443 (1991).
[31] A. Bergeon and E. Knobloch, "Natural doubly diffusive convection in three-dimensional enclosures," Phys. Fluids **14**, 3233–3250 (2002).
[32] D. Henry and H. Ben Hadid, "Multiple flow transitions in a box heated from the side in low-Prandtl-number fluids," Phys. Rev. E **76**, 016314 (2007).
[33] A. Bergeon, K. Ghorayeb, and A. Mojtabi, "Double diffusive instability in an inclined cavity," Phys. Fluids **11**, 549–559 (1999).
[34] J. Burke, A. Yochelis, and E. Knobloch, "Spatially localized oscillating states in periodically forced dissipative systems," SIAM J. Appl. Dyn. Syst. **7**, 651–711 (2008).
[35] J. Knobloch and T. Wagenknecht, "Homoclinic snaking near a heteroclinic cycle in reversible systems," Physica D **206**, 82–93 (2005).
[36] H.-C. Kao and E. Knobloch, "Weakly subcritical stationary patterns: Eckhaus instability and homoclinic snaking," Phys. Rev. E **85**, 026211 (2012).
[37] Y.-P. Ma, J. Burke, and E. Knobloch, "Defect-mediated snaking: A new growth mechanism for localized structures," Physica D **239**, 1867–1883 (2010).
[38] O. Batiste, E. Knobloch, I. Mercader, and M. Net, "Simulations of oscillatory binary fluid convection in large aspect ratio containers," Phys. Rev. E **65**, 016303 (2001).
[39] O. Batiste, E. Knobloch, A. Alonso, and I. Mercader, "Spatially localized binary-fluid convection," J. Fluid Mech. **560**, 149–156 (2006).
[40] Z.-W. Chen, J.-M. Zhan, Y.-S. Li, Y.-Y. Luo, and S. Cai, "Double-diffusive buoyancy convection in a square cuboid with horizontal temperature and concentration gradients," Int. J. Heat Mass Transfer **60**, 422–431 (2013).